+ESTRELIA
Safe Batteries with power

D1.3 Publishable summary

Lead Beneficiary: AMS

FP7-2011-ICT-GC

Project # 285739

Table of Contents

1. Final publishable summary report

The ESTRELIA platform developed during the last 3 years enables a significant advancement of the technology capabilities for battery management systems BMS design: It provides building blocks with enhanced reliability and safety at lowered costs for smart energy storage for FEVs. This is accomplished by proposing a modular approach with ultra capacitor power packs with higher density with 50% energy advantage.

Cycling test of the power pack consisting of the new ultra capacitors supplied by Corning and the Li-Ion energy pack provided by E4V have shown that high current power demand can be overtaken by the ultracapacitors and thus relieving the Li-Ion battery which can be monitored by lower thermal stress.

The new BMS ICs AS8506 from ams AG provides for the first time a flexible active cell balancing chip set also suited for the high accuracy demanding monitoring of Li-Ion batteries. The AS8506 Cell Monitor and Cell Balancer IC enables autonomous cell balancing, simultaneous cell voltage comparison and simplified readout of cells all in a robust, simple and small solution. It features simultaneous cell voltage comparison with upper and lower threshold, active- or optionally passive cell balancing by simultaneous comparison of actual cell voltages with a target cell voltage. Cells which are below target will either cyclically receive charge packages from an isolated DCDC converter or, optionally, cells above target will cyclically be discharged by an external resistor through integrated switches in an autonomous way.

The excellent functionality of this BMS monitoring and balancing concept has been demonstrated in this project in combination with Li-Ion batteries as well as with ultra capacitor power packs.

Tests with newly developed HV-test equipment have proven test isolation protections in the environment of several 100's V as present in FEVs. So the demonstration of a newly developed precision HV-attenuator enable also integrated solutions for accurate voltage measurements.

New safety sensors which are based on silicon based MEMS approaches deliver enhanced safety functions at lowered cost compared to existing solutions.

Test with abuse of Li-Ion cells have shown showed that it is possible to detect gas emissions a sufficient time span before a thermal runaway occurs. The gas sensor can detect a rise in volatile organic compounds VOC concentration even before a bloated cell fully opens. The measurements showed that this time span is, dependent on cell temperature and cell current, in the range of tens of seconds to several minutes. This time span is more than sufficient to take measures to avoid a thermal runaway of the battery.

While the gas sensor allows detection of very low levels of volatile organic compounds as emitted in thermal overruns of battery packs, the new spark detector concept based on cost effective MEMS/NEMS technology from CEA LETI enables general safety functions by flame detection from all hazardous events in a FEV.

Finally the development of new actuators as low cost power antifuse together with the new energy management HW (BMS IC) and SW from FhG IISB enables dynamic reconfigurable topologies for the energy storage unit, thus still enabling the functionality of the FEV despite single failing cells.

Find more information on: www.estrelia.eu

2. Summary description of project context and objectives

High costs together with concerns for driving range, reliability and safety have been the main hindrance for market adaption of full electrical vehicles (FEVs). ESTRELIA was an EU funded Green Car Initiative project where 9 strong partners worked on the major goal to provide increased performance of building elements at reduced costs for energy storage in FEVs. The project outcome provides cost efficient solutions to set industry standards and mass production.
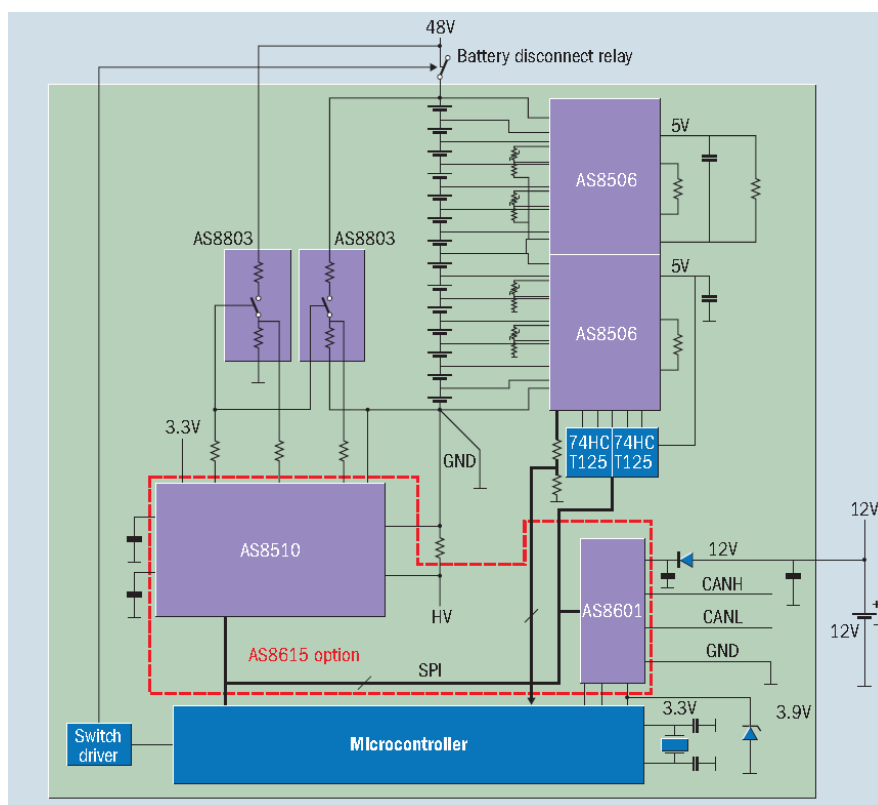
ESTRELIA has developed new IC devices, sensors and actuators to enable enhanced reliability and safety at lowered costs for smart energy storage in FEVs.
This was accompanied by a modular approach with ultracapacitor power packs provided by Corning delivering higher energy density and assembled by Valeo with integrating the new BMS ICs in the battery management electronic.
The BMS IC concept provides for the first time a flexible active cell balancing chip set suited also for the high accuracy required for Li-Ion batteries. This enables higher efficiency by lower energy loss and improved long term reliability at lower electronic component costs for Li-Ion energy packs.
To verify the functionality of this new BMS monitoring and balancing concept has been demonstrated in this project in combination with Li-Ion batteries as well as with ultra capacitor power packs. Newly developed BMS concepts and boards developed by Valeo enabled further functional verification in cooperation with the parallel FP7 Green Car Initiative project SuperLIB.

A new BMS ICs AS8506 based on a new concept in the HV-technology enhances the modularity of Li-Ion batteries as energy packs. For the first time provide a flexible active cell balancing chip set also suited for the high accuracy demanding monitoring of Li-Ion batteries. The AS8506 Cell Monitor and Cell Balancer IC enables autonomous cell balancing, simultaneous cell voltage comparison and simplified readout of cells all in a robust, simple and small solution. The AS8506 features simultaneous cell voltage comparison with upper and lower threshold, active- or optionally passive cell balancing by simultaneous comparison of actual cell voltages with a target cell voltage. Cells which are below target will either cyclically receive charge packages from an isolated DCDC converter or, optionally, cells above target will cyclically be discharged by an external resistor through integrated switches in an autonomous way.

Fig. 1: Application of the new AMS BMS ICs for 48V Li-Ion batteries
(from: http://www.newelectronics.co.uk/image-store/articles/56462%5CP21-22.pdf)

Tests with newly developed HV-test equipment by project partner Active Technologies have proven test isolation protections in the environment of several 100's V as present in FEVs. So the demonstration of a newly developed precision HV-attenuator enable also integrated solutions for accurate voltage measurements.

Beside monitoring of electrical and thermal parameters of energy storage cells additional safety and reliability monitoring is provided by new safety sensors. Gas emission sensors and flame detection sensors have been developed in this project permitting general safety functions for all hazardous events in a FEV.

New innovative sensors are required to ensure safety improvement for the usage of Li-Ion batteries. Ultra-sonic MEMS sensors have been developed by CEA-LETI to detect the sparks that can occur in case of damaged connections in Li-ion batteries. The detection principle is based on the acoustic emission of the arc.
The new MEMS based ultra-sonic sensors were designed, and a process flow was adapted from an inertial sensors process flow to fabricate theses sensors.
The ultra-sonic MEMS sensor capacity to be used for spark detection was also studied. First, commercial MEMS sensors were integrated and tested. Therefore an electronic interface was designed for signal acquisition, and the ARMA spark detection model matched with these

new MEMS & electronics. Tests in an electric car with a battery module generating sparks on demand proved the capability of MEMS sensor to achieve spark detection. The reliability of the detection device should be further enhanced with the ultra-sonic MEMS sensor developed during the project.

The gas sensor developed by AppliedSensor has been integrated to E4V's Li-Ion battery pack and monitors changes of combustible gases in battery cycling experiments. In all experiments the sensor showed a stable baseline and gas sensor signals were below 3,000 [a.u.] all the time and below the alarm threshold level of 12,000 [a.u.].

AppliedSensor started the project with the BEM-100 gas sensor module and introduced a smaller version in 2013. At the end of the project period a low power version (88% power saving compared to BEM-100) is now available. The small size and reflow capability allows easy integration as SMD component to the BMS electronics inside battery packs.

Besides its high sensitivity to hydrogen the sensor reacts to a wide range of VOCs. While it is very difficult for standard battery monitoring to detect cell leakage, the gas sensor reacts to VOCs from electrolyte and will alarm the BMS.

Within ESTRELIA novel antifuse power devices were developed and investigated. The development was mainly focused on two types of devices: An active triggered antifuse, which needs a controller to "blow"; and a passive diode-based antifuse. The active triggered antifuse is based on reactive nanolayers that release thermal energy when activated. The advantage of this principle is that the antifuse can be triggered externally. The reactive nanolayer stacks were designed and fabricated at Fraunhofer IISB. A buildup methodology was developed and the resulting devices were characterized. Further a novel type of a passive antifuse has been developed and characterized. Different concepts of antifuse devices were investigated in consideration of their applicability to satisfy the specifications defined. The result of this research is a passive antifuse based on the spiking of aluminum through the pn-junction of a semiconductor diode. Because the aluminum spiking process is difficult to simulate, the phenomenon was investigated directly by real semiconductor process runs. After completion of this research the final device was fabricated and characterized. A demonstrator housing as well as the interconnect design was simulated, optimized and subsequently fabricated. The very ambitious and challenging targets of almost 1mΩ on-resistance and 100A continuous current set at the beginning of the project have been fulfilled successfully.

The novel antifuse power devices have the potential to significantly increase the reliability of battery systems. Together with the new energy management HW (BMS IC) and SW provide dynamic reconfigurable topologies for the energy storage unit it still enables the functionality of the FEV despite single failing cells.

E4V, a major actor in the electric vehicle market as a Lithium battery supplier, develops batteries including the battery management system hardware and embedded software. Battery management ICs are strategic components regarding the integrity of the battery monitoring system, and their integration is complex too. The ESTRELIA project was a good opportunity for E4V to test the new battery monitoring IC provided from AMS.

The integrity of the system can also be improved with new kind of sensors, and one of ESTRELIA's main objective is to integrate and tests new sensors in a Lithium battery.

To support the development of semiconductor manufacturing technology for BMS ICs, Fraunhofer IISB simulated ball bonding processes on thick isolation structures. Setting up of the simulation included some 1000 vias between the bonding pad and an underlying metal layer that was supposed to act as a crack stop layer. To obtain the materials parameter of the gold bonding ball, nanoindentation measurements were performed and evaluated. In addition, ultrasonic softening was included for the side-to-side movement during the bonding after the initial squashing of the bonding ball against the bonding pad. After the shape of the ball after bonding was obtained correctly in the simulation, the methodology was used to investigate technological options like alternative bonding processes and whether the intermediate metal layer could be safely removed.

3. Description of the main S&T results/foregrounds

The ESTRELIA platform which has been developed during the last 42 months enables a significant advancement of the technology capabilities for battery management systems design: ESTRELIA provides building blocks with enhanced reliability and safety at lowered costs for smart energy storage for FEVs. This is accomplished by proposing a modular approach with ultra capacitor power packs with higher density with 50% energy advantage. Cycling test of the power pack consisting of the new ultra capacitors supplied by Corning and the Li-Ion energy pack provided by E4V have shown that high current power demand can be overtaken by the ultracapacitors and thus relieving the Li-Ion battery which can be monitored by lower thermal stress.

Battery Monitoring and Balancing ICs

A new BMS ICs AS8506 based on a new concept in the HV-technology enhances also the modularity of Li-Ion batteries as energy packs. For the first time provide a flexible active cell balancing chip set also suited for the high accuracy demanding monitoring of Li-Ion batteries. The AS8506 Cell Monitor and Cell Balancer IC enables autonomous cell balancing, simultaneous cell voltage comparison and simplified readout of cells all in a robust, simple and small solution. The AS8506 features simultaneous cell voltage comparison with upper and lower threshold, active- or optionally passive cell balancing by simultaneous comparison of actual cell voltages with a target cell voltage. Cells which are below target will either cyclically receive charge packages from an isolated DCDC converter or, optionally, cells above target will cyclically be discharged by an external resistor through integrated switches in an autonomous way.


**Fig. 1: Active cell balancing concept illustrated for 7 cells**

Key Features

- Simultaneous cell voltage capture for balancing and SOA monitoring
- Autonomous balancing and SOA monitoring strongly reduces data communication and data processing and thereby improves EMC robustness
- Active charge balancing with very few external components for good efficiency and little heat dissipation.
- Absolute cell voltage readout for OCV capture and cell impedance calculation. Readout of 2 temperature sensors

Key Benefits

- recover capacity loss of batteries, increase operating time, as well as improve overall system run time.
- tremendously reduced communication saving costs in the system and making the system more reliable
- active balancing is possible as an as an energy efficient option
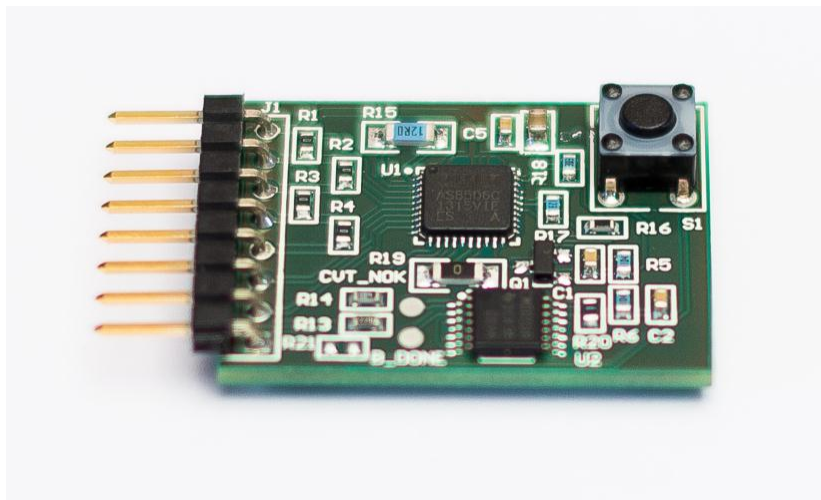
Fig. 2: AS8506 BMS IC demo board for autonomous cell supervising and active or passive cell balancing function
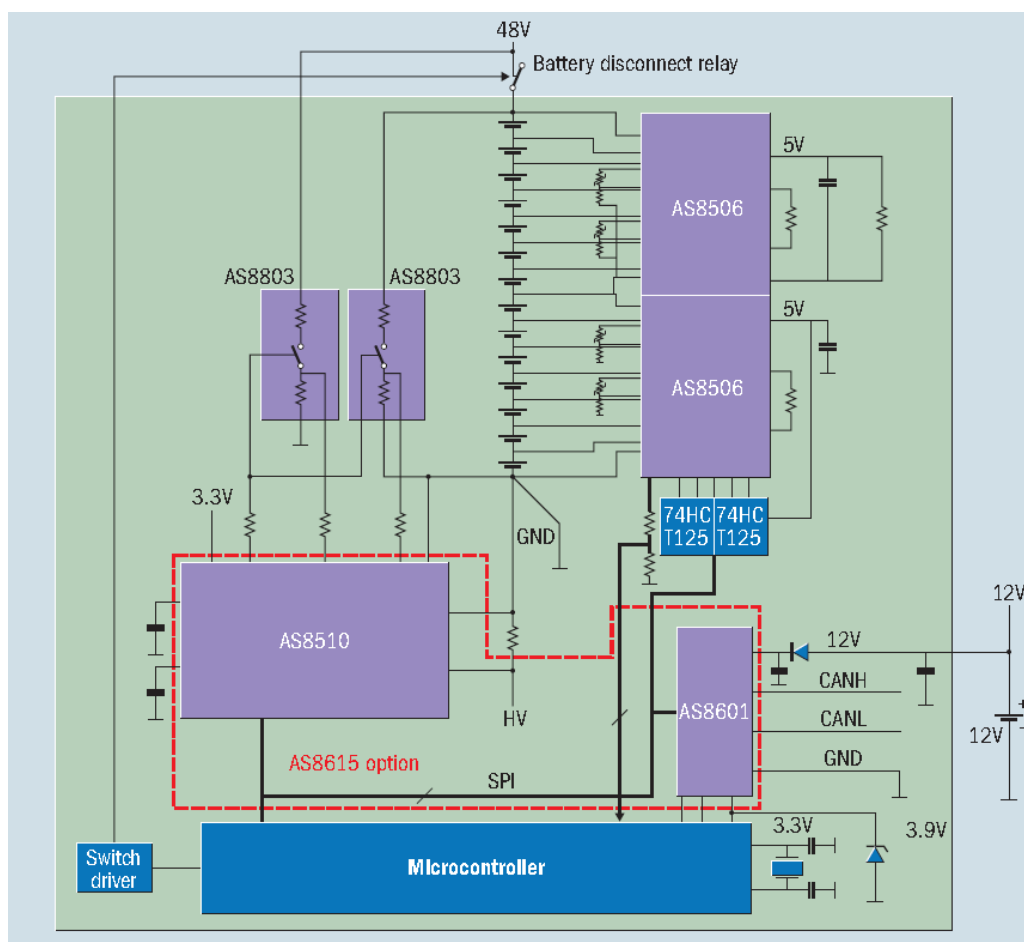
Fig. 3: Application of AMS BMS ICs for 48V Li-Ion batteries[1]

Energy Storage Pack Integration

The excellent functionality of this BMS monitoring and balancing concept has been demonstrated in this project in combination with Li-Ion batteries as well as with ultra capacitor power packs.

Tests with newly developed HV-test equipment by project partner Active Technologies have proven test isolation protections in the environment of several 100's V as present in FEVs. So the demonstration of a newly developed precision HV-attenuator enable also integrated solutions for accurate voltage measurements.

The gas sensor developed by Applied Sensor was tuned for an electrical vehicle application during the ESTRELIA project, and was tested in real condition, in the energy demonstrator pack. During the characterization of the prototype, the sensor detected changes in readings due to the temperature, not because of errors in the sensor itself, but because VOCs are more

---

[1] http://www.newelectronics.co.uk/image-store/articles/56462%5CP21-22.pdf

volatile and as such increase concentration when the temperature is increased. At the maximum temperature during characterization tests, around 40°C (close to the maximum battery temperature of 45°C), the PWM value of the sensor reported a maximum value of 15%, and showed enough margin regarding the threshold of gas detection of 50%. So the gas sensor developed by Applied Sensor in ESTRELIA is compatible with the use in a vehicle application.

The combination of the energy pack with the ultracapacitor "power pack" demonstrator was realized on a simulation basis within the ESTRELIA project. In cooperation with FP7 project SuperLIB a common test cycle was defined with the ARTEMIS urban cycle demanding higher power from energy storage unit. The Li-Ion energy packs was tested based on this ARTEMIS cycle profile to show possible impact of this combination. The result of such a combination is positive regarding the temperature increase, which is lower on the profile tested when an ultracapacitor is used to supply the power peaks. The temperature of the battery increases at a rate of 2.2°C/hour without ultracapacitor, and 2°C/hour when an ultracapacitor is used. The improvement of such a combination was low for such profile, which is already an aggressive profile regarding power peaks. In conclusion, the addition of a power pack in combination with the energy pack is hardly justified with a thermal performance criterion.

There may be possibility for lower system cost due to fewer Li-Ion packs required to support the peak currents required in the small case example studied. In the decomposed cycle the peak current required by the energy pack in charge and discharge are potentially lowered, when compared to the full profile. The peak current exceeds 60Amp for the full profile, while it requires a maximum of 35 Amp for the decomposed cycle. Since the Energy pack has peak current limitations, the used of the Power pack could allow a lower scaling factor instead of and hence lower number of energy packs for the same application. This could lower the system cost due to the number of energy packs required.

Battery Emission Gas Sensor

The gas sensor developed by AppliedSensor to monitor emissions from battery packs has been integrated to E4V's Li-Ion demonstrator to monitors changes of combustible gases in battery cycling experiments. In all experiments the sensor showed a stable baseline and gas sensor signals were below 3,000 [a.u.] all the time and below the alarm threshold level of 12,000 [a.u.].


Fig. 4: Gas Sensor evaluation kit

AppliedSensor started the project with the BEM-100 gas sensor module and introduced a smaller version in 2013. At the end of the project period a low power version (88% power saving compared to BEM-100) is available. The small size and reflow capability allows easy integration as SMD component to the BMS electronics inside battery packs.

Fig. 5: Evolution of gas sensor size over the project period

Signals from temperature cycling are small compared to signals from cell abuse tests and it is concluded that the observed high signals measured are caused by small amounts of hydrogen being released when batteries reach a critical state. Sensor signals observed in charging-discharging-cycles showed only small signals far below the alarm threshold limit.
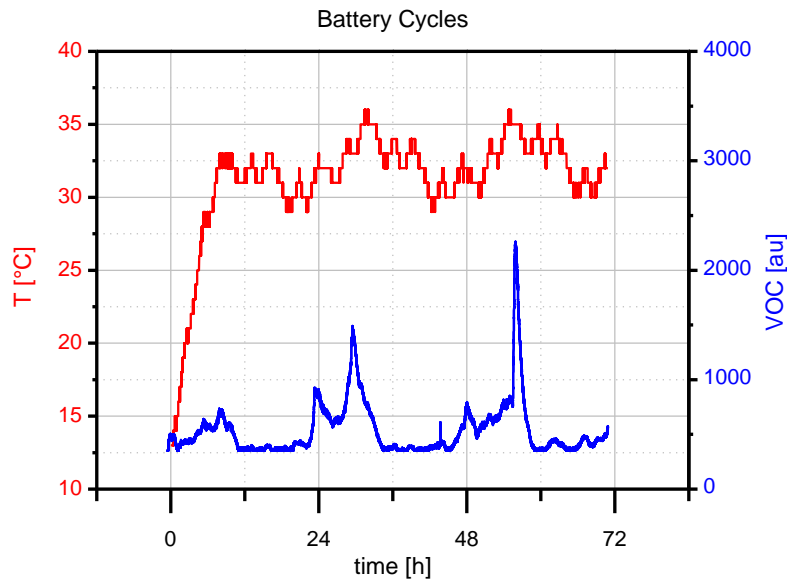
Fig. 6: Gas sensor signals at charging-discharging-cycles of a battery pack.

In overcharging experiments at Fraunhofer IISB cell leakage could be detected even before a bloated cell fully opened and time span was sufficient to prevent a thermal runaway. Since hydrogen concentrations below 50ppm could not be measured with the reference sensor (Crowcon Gasman, 0-2000ppm) the sensor was calibrated using hydrogen. The calibration curve reaches the sensor alarm threshold at 27ppm of hydrogen, this is less than a thousandth of the lower explosive limit.
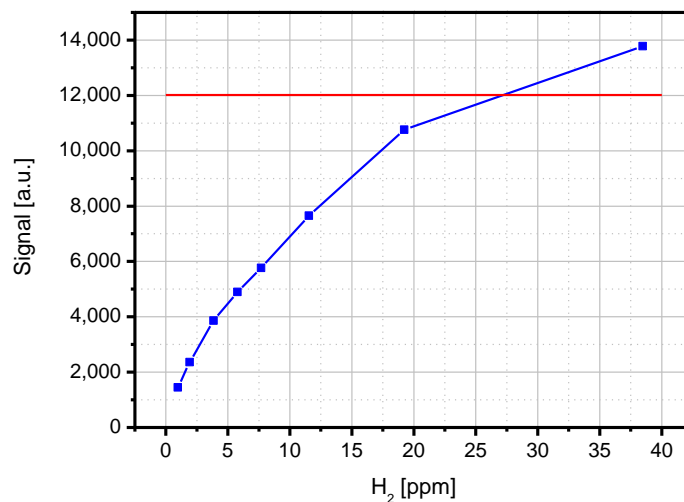
Fig. 7: Gas Sensor calibration curve for hydrogen

Besides its high sensitivity to hydrogen the sensor reacts to a wide range of VOCs. While it is very difficult for standard battery monitoring to detect cell leakage, the gas sensor reacts to VOCs from electrolyte and will alarm the BMS.[2]
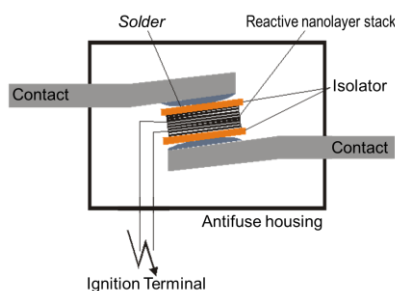
Active Antifuse

In normal operation, the active antifuse behaves like an isolator which prevents current flow. In case of a faulty battery cell, the device can be irreversible switched to a low resistive state by an external signal, provided e.g. from the battery management system. The formation of many intermetallic compounds, for example SiTi, can provide a strongly exothermic reaction. This reaction can be used to generate high temperatures for a very short time, destroying an isolator layer and welding the antifuse contacts together. Figure 8. shows the principle of the reaction of nanoscale multilayers.
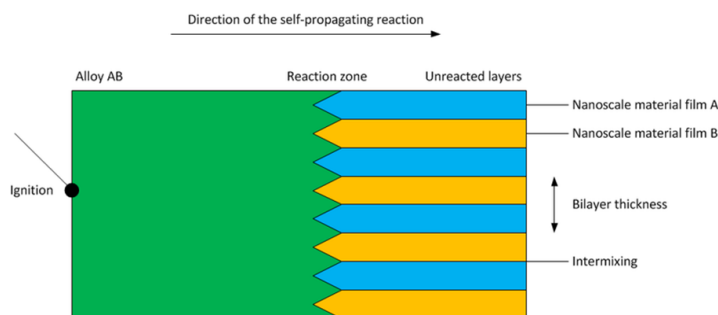
Fig. 8: Principle of the reaction of a nanolayer stack

A basic schematic drawing of the device is shown in figure 9. A preliminary wiring symbol of the active antifuse is depicted in Figure 10.

Fig. 9: Principle schematic of the active nanolayer Antifuse (source Fraunhofer IISB)
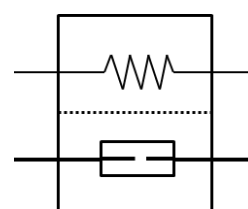

Fig. 10: Wiring symbol of the active Antifuse (source Fraunhofer IISB)

Figure 11 shows a test setup of the active antifuse device. The setup consists of two copper terminals, isolation layers and a nanolayer stack. The diagram in Figure 12 depicts the resistance of some active antifuses before and after their ignition. The ignition was initiated

[2] Investigation of gas sensing in large lithium-ion battery systems for early fault detection and safety improvement
M. Wenger[1], R. Waller[1], V.R.H. Lorentz[1], M. März[1], M. Herold[2]
[1] Fraunhofer IISB, Erlangen, Germany [2] AppliedSensor GmbH, Reutlingen, Germany
IECON'2014 Dallas, TX, USA from October 29-November 1, 2014

by an electrical pulse. It can be seen that resistance values below the targeted value of 1mΩ have been reached.
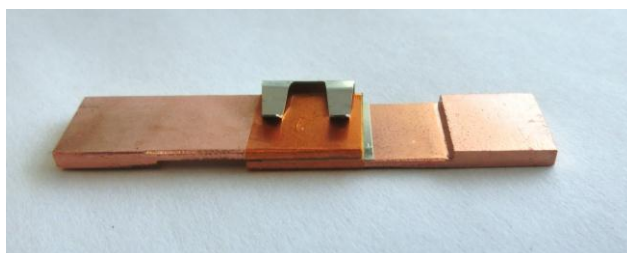
**Fig. 11: Test setup of an active antifuse device (source Fraunhofer IISB)**
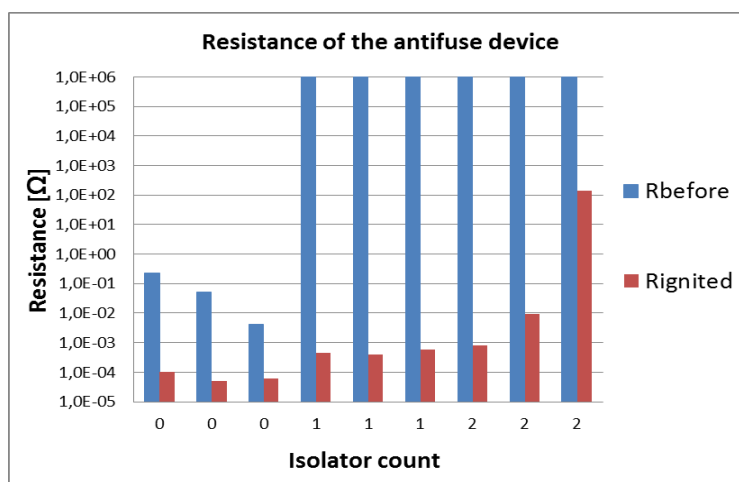
Fig. 12: Resistance of active antifuse devices before and after ignition (source Fraunhofer IISB)

The active triggered antifuse is based on reactive nanolayers that release thermal energy when activated. The advantage of this principle is that the antifuse can be triggered externally. The reactive nanolayer stacks were designed and fabricated at Fraunhofer IISB. A buildup methodology was developed and the resulting devices were characterized. Values which meet the requirements mentioned before were successfully reached.

Passive Antifuse

The novel passive antifuse device, presented here, is intended for bypassing energy sources, especially sources which can change their polarity in case of failure. When the resistance of a battery cell rises significantly, the polarity of the cell reverses and causes current to flow through the diode of the antifuse. This sequence is visualized in Figure 13. The current through the diode causes it to heat and change its behavior irreversible to a low resistive contact.
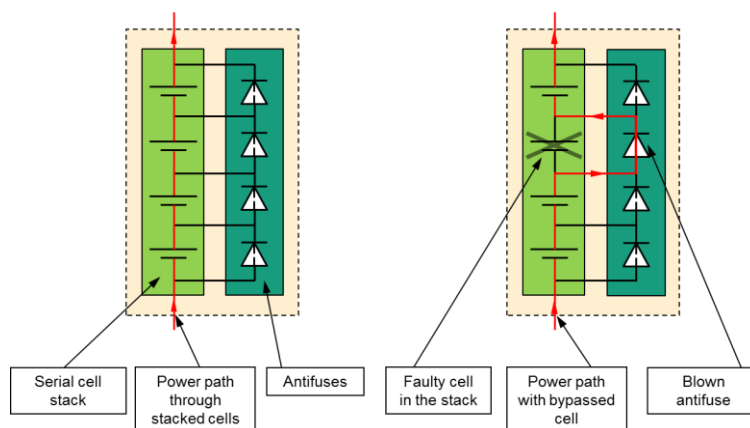
Fig. 13: Illustration of the passive antifuse activation and bypass mechanism
(source Fraunhofer IISB)

The passive antifuse behaves like a rectifying contact which prevents current flow in its initial state and forms a high current bypass in its activated state. In case of a faulty battery cell, the reverse biasing voltage causes high currents flowing through the diode as a consequence of the increased series resistance of the faulty battery cell. The resulting heating of the antifuse device induces spiking and is thus forming a low resistive symmetrical conductor which then bypasses the defective battery cell. The underlying physical effect is the spiking of aluminum in silicon. Figure 14 shows a schematic drawing as well as a REM photograph of an aluminum spike penetrating a pn-junction.
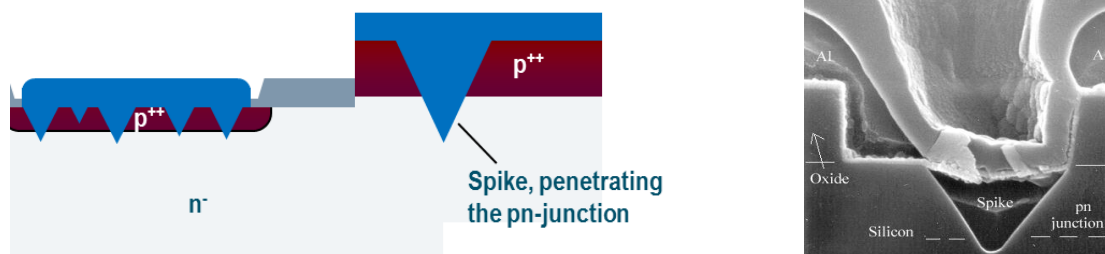
Fig. 14: Aluminum spike penetrating a pn-junction

To verify the thermally improved design of the assembly, the setup was simulated with ANSYS. A housing of the device was incorporated in the simulation model in order to consider the thermal influence of this housing. A screenshot of the simulation results is depicted in Figure 15. Due to the fact that the spiking process cannot be simulated with state-of-the-art simulation tools, the simulated temperature distribution of the antifuse chip is only an approximation.
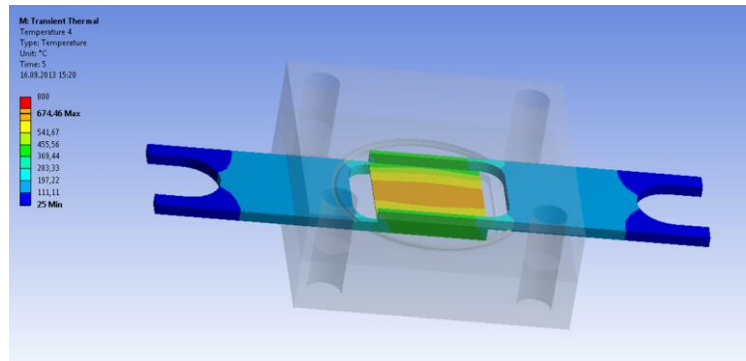
Fig. 15: Simulated temperature distribution of the antifuse buildup including the housing (source Fraunhofer IISB)

A photography of the assembled antifuse in a housing of K-Therm® AS 600 M compound as well as the preliminary wiring symbol of the passive antifuse is shown In Figure 16 the antifuse demonstrator is displayed with a top of polycarbonate for better visibility.


Fig. 16: Assembled antifuse device with a top of polycarbonate for better visibility (source Fraunhofer IISB)

Several antifuse chips were activated within the demonstrator housing and subsequently the resulting resistances of the devices measured. First, the voltage drop of the samples was measured at 2A and 5A, and then the devices were activated with 100A for 10 seconds. Afterwards the chip resistances were measured with 2, 5, 10, 50 and 100A in forward as well as in reverse direction. The activation and measurement procedure versus time is depicted in Figure 17.
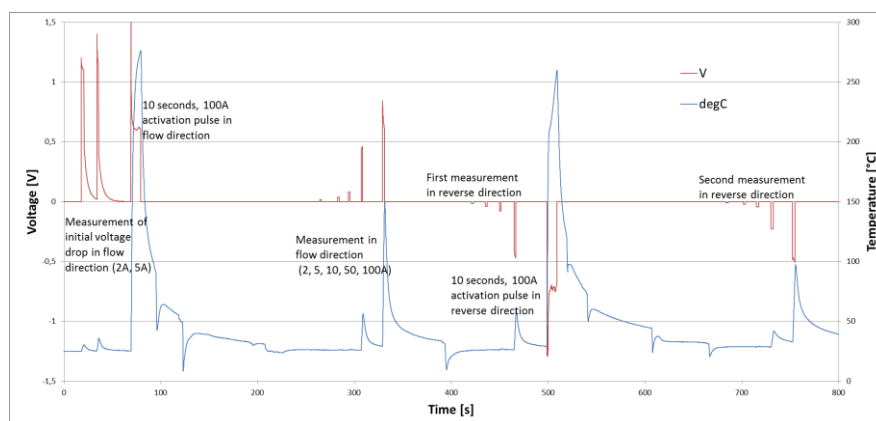
Fig. 17: Activation and measurement procedure versus time (source Fraunhofer IISB)

The results of the measurements are shown in Figure 18. The final resistance of the devices is in the range of 4 to 5mΩ which is about 5 times higher than the targeted value of less than 1mΩ. This leads to a power dissipation of 40 to 50W at 100A. The heat generation occurred mainly in the regions near the contact areas. A part of this heat generation in the contact zones is due to the contact resistance and the aluminum sheet resistance on the chip surface. The aluminum sheet resistance contributes with about 1.8mΩ (calculated value) to the overall resistance, whereas the contact resistance contributes with about 3.5mΩ (measured value) to the overall resistance of the samples.
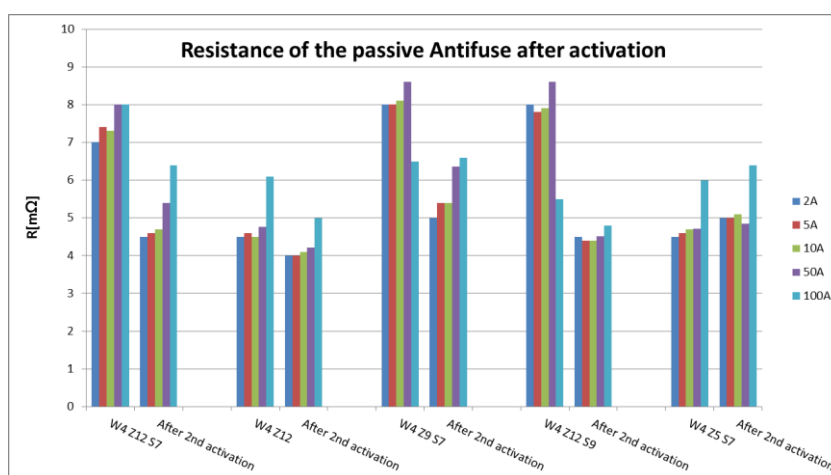
Fig. 18: Bar chart of passive antifuse resistance measurements after activation (source Fraunhofer IISB)

A novel type of a passive antifuse has been developed and characterized. First, different concepts of antifuse devices were investigated in consideration of their applicability to satisfy the specifications defined. The result of this research was beside the active antifuse a passive antifuse based on the spiking of aluminum through the pn-junction of a semiconductor diode. Because the aluminum spiking process is difficult to simulate, the phenomenon was investigated directly by real semiconductor process runs. After completion of this research the final device was fabricated and characterized. A demonstrator housing as well as the interconnect design was simulated, optimized and subsequently fabricated.
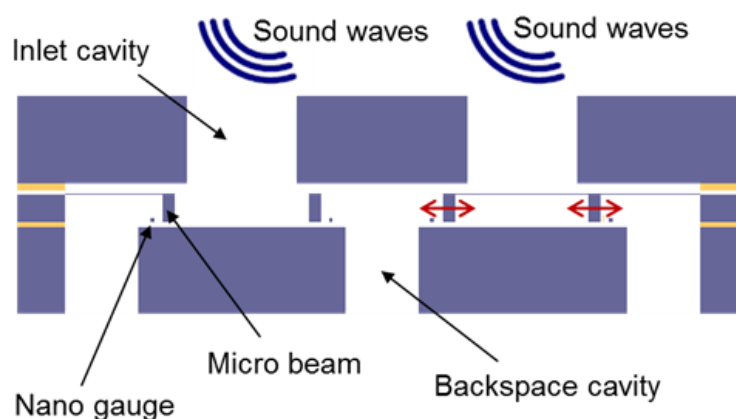
Spark Detection Sensor

A new spark detection sensor based on MEMS was developed during the ESTRELIA project, as an additional safety improvement for the usage of Li-Ion batteries.

The ultra-sonic MEMS sensors are developed to detect the sparks that can occur in case of damaged connections in Li-ion batteries. The micromachined sensors target characteristics have been defined in the specifications of WP2.

The experimental study of the acoustic arc generation, propagation in the air and signature leads to a 20 kHz-300 kHz frequency bandwidth specification for these sensors. While classical MEMS microphones enable to measure only in the audible bandwidth (below 20

kHz), MEMS CMUTs target frequencies typically higher than 1MHz. There is therefore a gap in the 20 kHz-300 kHz bandwidth needed by the spark detection application. After an introductive state of the art, a pre-dimensioning of the sensor has been carried out, leading to the choice of a MEMS piezo-resistive planar microphone technology.


Fig. 19: Schematic cross section of the spark detection sensor

The ultra-sonic MEMS sensor is based on a new concept of MEMS sensors developed at CEA-Leti to manufacture inertial sensors. Its structure is made of 4 beams moving within the plane of the substrate when subjected to a force due to propagation of pressure wave (Fig. 19). Cavities in top and in bottom wafers are used as sound entrance and backspace cavity respectively. Small slits between the beams and top and bottom wafers enable the motion of the beams while ensuring pressure drop from one to the other side of the beam. The stress induced by the motion of a beam inside suspended piezo-resistive Si nano-gauges is transduced into resistance variations and measured by use of Wheatstone bridge architecture.

Coupling sound pressure propagation and electro-mechanical behaviour of the sensor enabled us to determine the sensor response and to establish proper dimensions of the mechanical parts and acoustic network to fulfil the specifications in terms of bandwidth, sensitivity and resolution. With limited footprint of 1.5mm², this sensor provides high sensitivity in spite of the high stiffness required by the large bandwidth. Expected sensitivity is 46 µV/Pa @ 100 kHz and expected resolution is 0.23 mPa/√Hz (0.1 Pa for the bandwidth of 300 kHz). Optimisation rules are proposed to enhance the properties of the final design.

The technological process is based on an M&NEMS platform that was developed at CEA-Leti for inertial sensors. This process has been adapted to the ultrasonic sensor, and following the layout was drawn. The technological fabrication progress is described as well as the main issues encountered at sealing step and the associated proposed solutions. In-run characterisations results illustrate the different steps (Fig. 20).
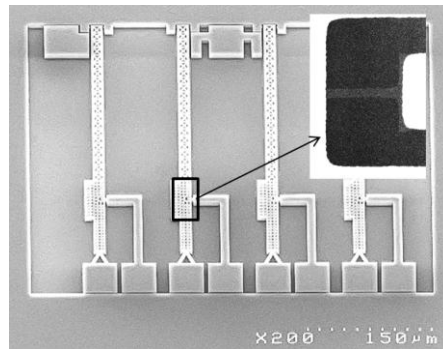
**Fig. 20: SEM picture of beams suspended on micro-hinges
(insert: zoom on the piezo-resistive nanogauge),**

The first processed sensor wafers are available (Fig. 21) and preliminary wafer-level test is ongoing.
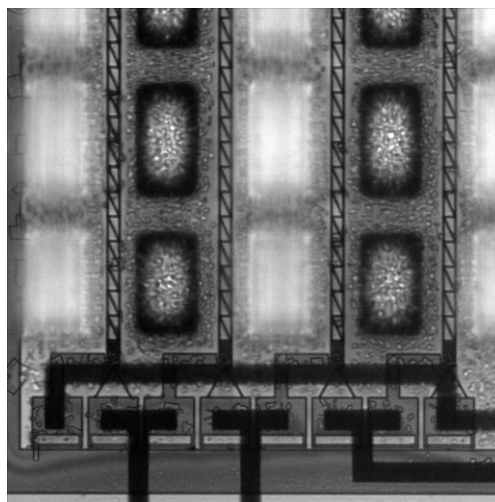
Fig. 21: Infrared picture of a fully processed ultrasonic sensor wafer (detail)

The innovative ultra-sonic MEMS sensor is to be integrated to achieve a spark detector for Li-ion batteries. Integration and tests are done to assess of the MEMS sensor capacity to be used for spark detection.

The sensor fabrication was delayed due to technological issues. To partially recuperate from the delay accumulated in the sensor fabrication the spark detection module was achieved with an alternative MEMS technology and based on commercial microphones. This permitted to evaluate the capacity of mems sensor to achieve spark detection requirements even if the selected commercial MEMS sensor had a reduced bandwidth.

The electronic interface was designed, the spark detection tested using dedicated detection algorithms, and finally the final test in an electric car was carried out (Fig. 22). These tests showed good results and permitted to prove the capacity of MEMS sensors to achieve spark detection. When the new ESTRELIA MEMS sensors will be available, the developed setups will be used with the same procedure to verify their functionality with respect to the target and to evaluate their advantages compared to the commercial sensors. The results obtained

with commercial sensors should be further enhanced with the new MEMS sensors, which were designed to obtain a larger bandwidth: following, the margin between the levels of correlation of arcing signature and noise, which is not sufficient with commercial sensors to ensure a good reliability of the detection device (Fig. 23), should increase.
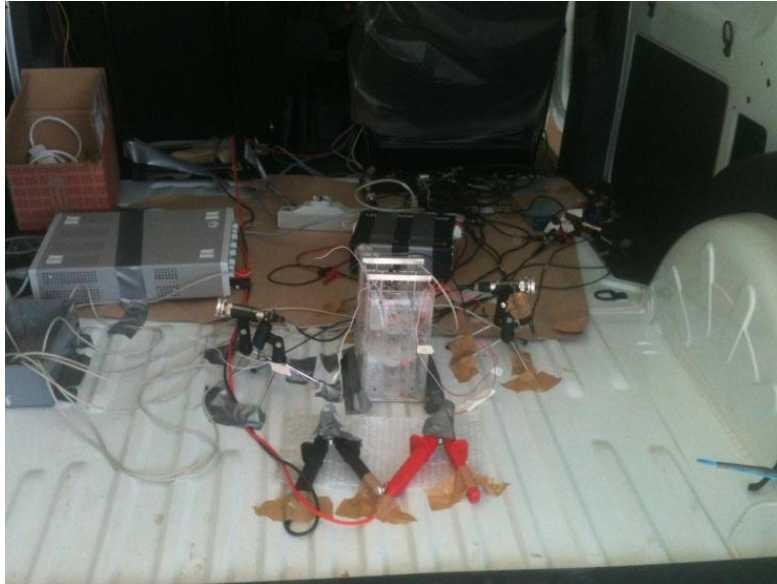

Fig. 22: experimental system in the boot of the Kangoo ZE
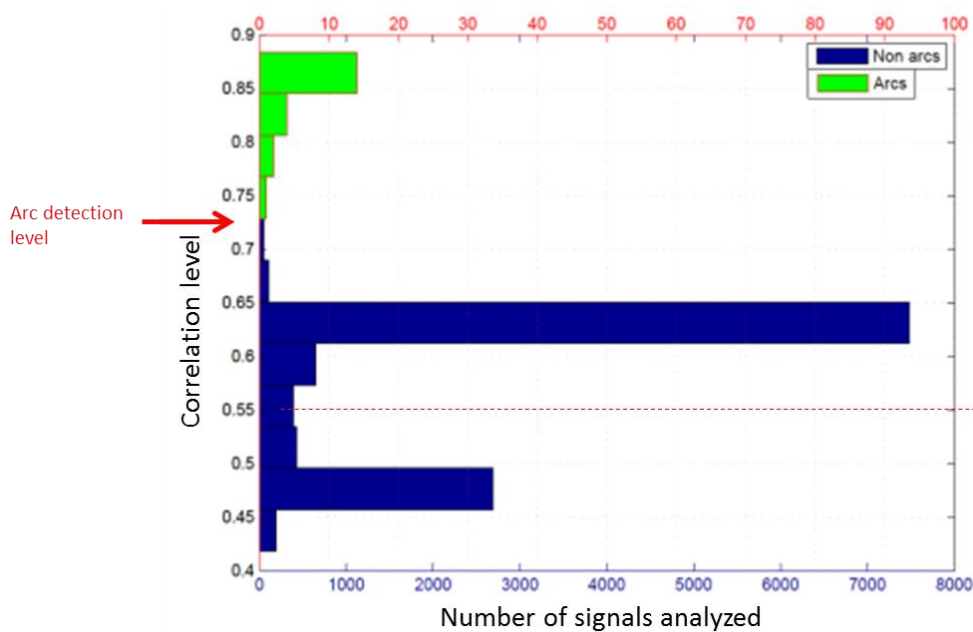
**Fig. 23: Final results of spark detection at Kangoo ZE driving test**

Advanced Technology Integration

Within ESTRELIA, IISB was to support the development of the BMS IC by performing TCAD simulations to investigate new technology concepts such as the use of thick oxides for high voltage isolation and their potential effects on reliability. For this purpose, IISB modelled a ball bonding process on part of the battery management system (BMS) IC incorporating thick oxide. The use of thick oxide for high voltage isolation raises the issue of crack formation during ball bonding processing, potentially leading to reliability issues. A 3D model was set-up of the device comprising a thin and a thick oxide layer. A ball bonding process was simulated upon the device to model the stresses induced into these layers, see Figure 24. The bond process involves the downward pressure of the bond tool to squash the ball against the bonding pad. After this impact stage, ultrasonic agitation is then added increasing the stress induced and further squashing the bonding ball, see Figure 25. A high number of vias are present in the structure between the bond pad and underlying metal layer, 1005 of which were simulated as shown in Figure 26. Preliminary results at this stage were shown at the EuroSimE conference.[3]


3D model of device in bonding process   Simulated stress in oxide layers
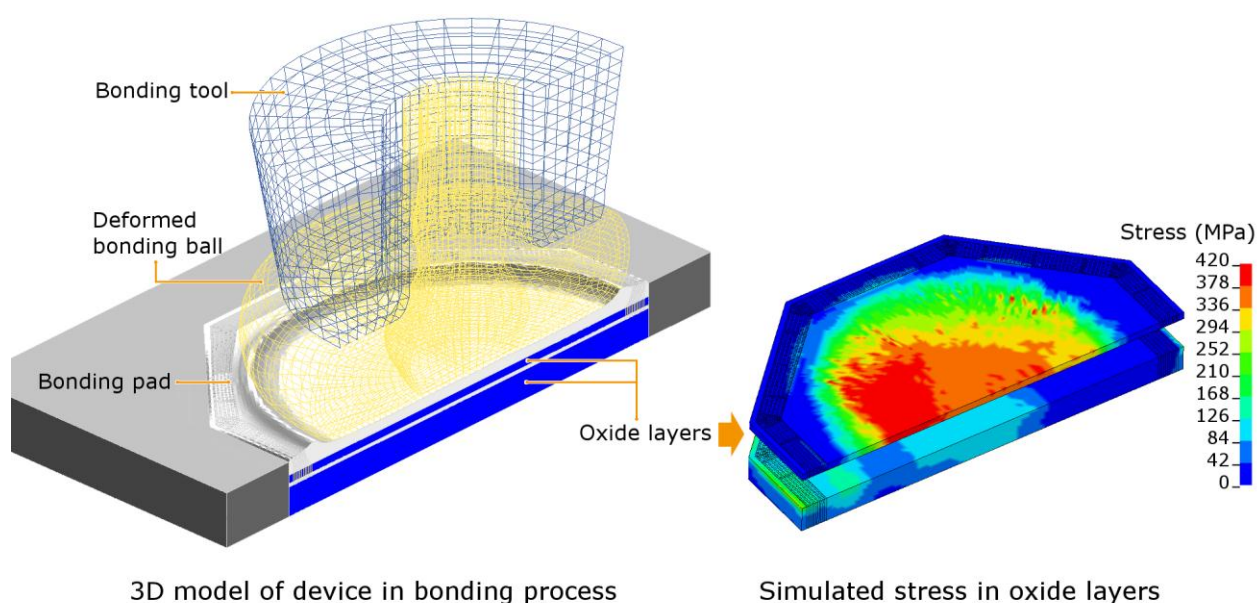
Fig. 24: 3D model of device undergoing a ball bonding process (left) to estimate the stresses induced into the oxide layers (right). The model is shown with deformed ball and splash shaped deformation of the bonding pad. Stress in the thin oxide layer exceeds the strength of the material (red). Stress in the thick oxide layer is low.

---

[3] A. Wright, S. Koffel, P. Pichler, H. Enichlmair , R. Minixhofer, E. Wachmann, Proceedings of the 14th EuroSimE, 2013, DOI: 10.1109/EuroSimE.2013.6529933.
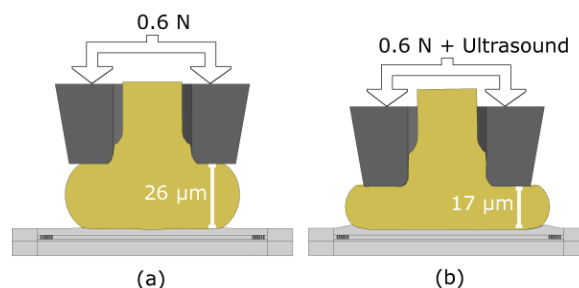
Fig. 25: Deformation after impact stage (a) and application of ultrasound (b). Amount of deformation is evaluated by the measurement of the ball height as shown.
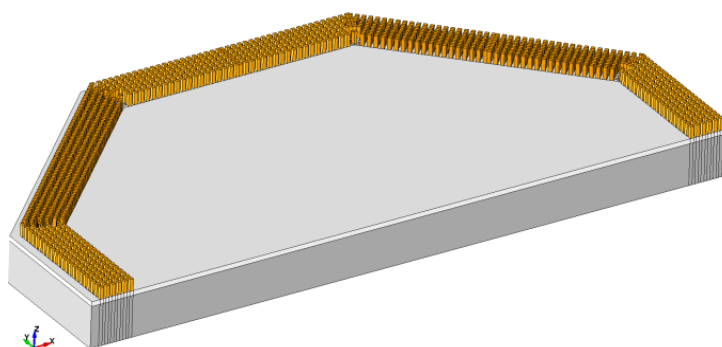

Figure 26: Inclusion of 1005 interconnect vias in the half-structure above the intermediate metal layer (white) and the thick oxide (grey).

In order to have the results of the simulation match reality as closely as possible it was desired to make measurements of the production geometry and the material parameters of the gold which are altered when it is melted into a ball. To measure the as-produced geometry, cross sections were made with the bonded ball over the isolation structure. Focussed ion beam preparation was used in conjunction with scanning electron microscopy followed by preparation of samples for optical microscopy (Figure 27). The dimensions of the isolation structure were measured and the simulation geometry was then adapted to match. Crucially, the amount the balls deformed during manufacturing was also determined from cross sections. This allowed the simulation to be calibrated to model the equivalent deformation and therefore better predict the stress induced into the lower layers. Lastly, the form of the bond tool's tip, also important in determining the stress distribution, was extracted from the imprint it left upon the bonded ball.
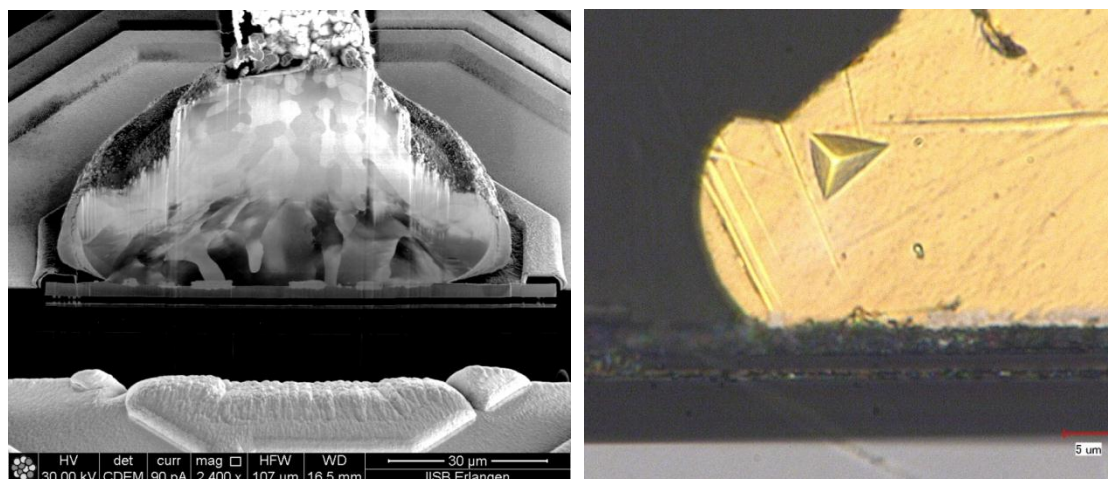
Fig. 27: (left) focussed ion beam cross section of the bonded ball over the as-produced IC, (right) optical cross section with nanoindent on the surface of the gold ball.

With the simulation geometry, and expected ball deformation known, attention was turned to obtaining the correct mechanical parameters for the bonded ball gold. These could not be taken from values of the gold feedstock wire for bonding, as mechanical properties are altered once the gold is melted into the bond ball (larger grains are formed). Therefore measurements and analysis were necessary to determine the mechanical properties, especially the harder to obtain plasticity properties. The gold bond ball is of small size at 60 μm in diameter, ruling out most conventional methods of measurement e.g. universal testing machines. Measurement was made possible by the use of a nanoindenter, which drove a small tip into the sample with nano-scale resolution. However, although the data collected by the nanoindenter readily provides information on the elastic properties of samples, it does not directly yield parameters of plasticity – necessary for this simulation. The solution to this came in the work of Ma et al.[4] where an analysis coupled with an additional measurement were used to extract the plasticity parameters of the yield point and strain hardening exponent from the nanoindenter data. The additional measurement required the use of an atomic force microscope to measure the topography of the nanoindent, see Figure 28.
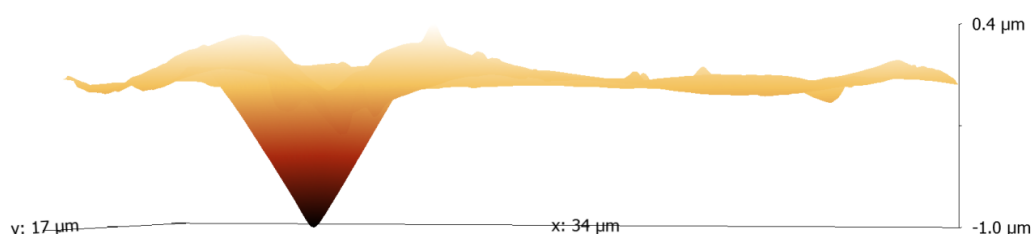

Fig. 28: Atomic force microscope cross section of a nanoindent made into the deformed gold ball

---

[4] Z. S. Ma, Y. C. Zhou, S. G. Long, X. L. Zhong, and C. Lu, Mechanics of Materials, vol. 54, pp. 113–123, 2012.

With the combined nanoindent and atomic force microscopy measurements entered into the dimensionless functions from Ma et al. elastic and plastic material parameters of the gold ball were obtained. These were then duly entered into the simulation model.

As indicated above, the bonding ball is first deformed during impact against the pad with a given force and squashed to a given height. Only upon the application of ultrasound does the ball deform further to its final bonded height. To simulate ultrasonic agitation, 60 cycles of ultrasonic motion were modelled combined with the effect of ultrasonic softening and additionally the friction was progressively increased to simulate the formation of the bond between ball and pad. To our knowledge this was the first time ultrasonic motion and softening had been simulated for such a process and the highest number of ultrasonic cycles simulated for such. The evolution of the deformed ball height per cycle and over the simulation time is shown in Figure 29. This showed the necessity of simulating a large number of cycles (compared to previous approaches in literature) as the deformation is significant over many cycles. Deformation was initially rapid over the first 10 cycles but reduced steadily so that it can be estimated from the height reduction per cycle that even the full number of 1200 ultrasonic cycles would not lead to a more significant squashing (Figure 29).
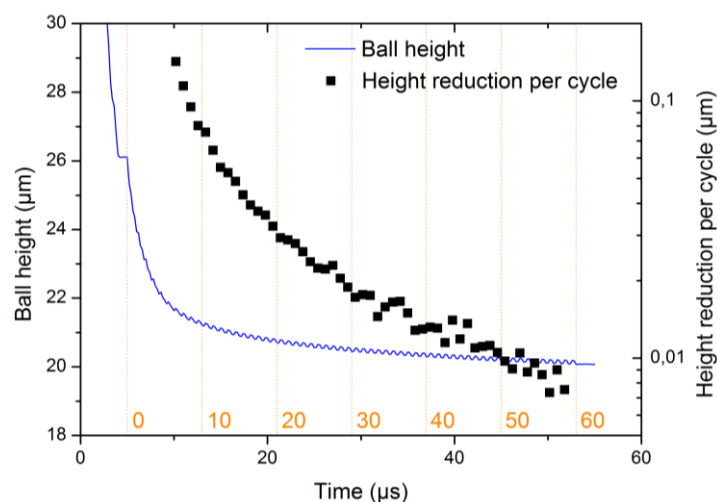

Fig. 29: Evolution of the height of the bonding ball during ultrasonic agitation for over 60 cycles. The numbers of cycles are indicated by number and dashed lines.

As mentioned above, 1005 vias were included in the simulation model. To assess their impact on the structure and possible increased induction of stress into the lower high voltage isolation oxide, simulations were made including them and with them absent. The results shown in Figure 30 indicate that the vias had only a localised effect and could therefore be neglected from further simulations allowing a speed up of the simulation time.
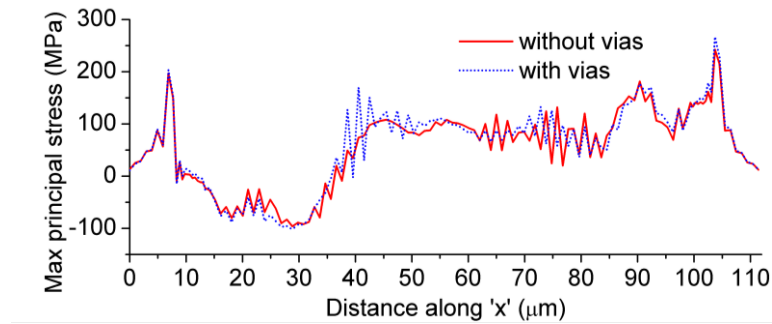
Fig. 30: Maximum principal stress at the top of the high voltage isolation oxide layer, and 7μm silicon either side. Stress is shown for the model with and without vias included.

During the project, the question arose whether the breakdown voltage of the bonding pad isolation could be increased by increasing the electrical separation between the bond pad and the silicon substrate by removal of metal layer 3. (Figure 31). However, the original purpose for metal 3 layer's existence was to provide a crack stop layer to prevent any oxide cracks beneath the bond pad from propagating further into the thick oxide. This raised the question of whether the removal of this protection layer, to improve electrical performance, would worsen the situation for the failure of the oxide.
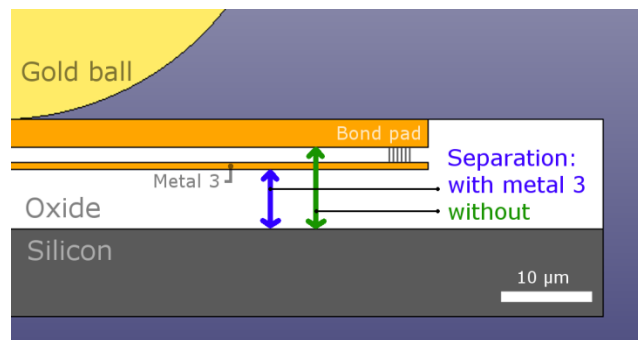
Fig. 31: Electrical separation between bond pad and silicon substrate with and without metal 3.

The results of the simulation were entered into the failure prediction model from Christensen.[5] This yielded the result shown in Figure 32. It can be seen that the failure predicted for both the presence and removal of metal 3 are quite similar, and both do not predict failure of the oxide. As no failure is predicted for the removal of metal 3, this work would suggest its safe removal. This would therefore allow an improvement of the electrical isolation, by improved separation.

---

[5] R. M. Christensen, J. Eng. Mater. Technol, vol. 129, no. 2, p. 173, 2007.
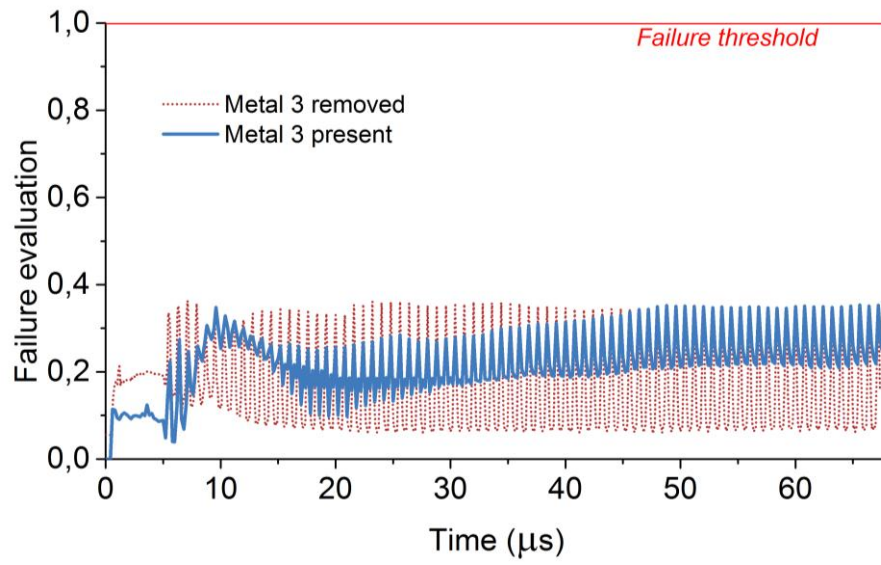
Fig. 32: Failure prediction with and without metal 3. No failure is predicted for metal layer 3's removal.